iScience

CellPress
OPEN ACCESS

Article

Neuropeptidergic regulation of neuromuscular signaling in larval zebrafish alters swimming behavior and synaptic transmission

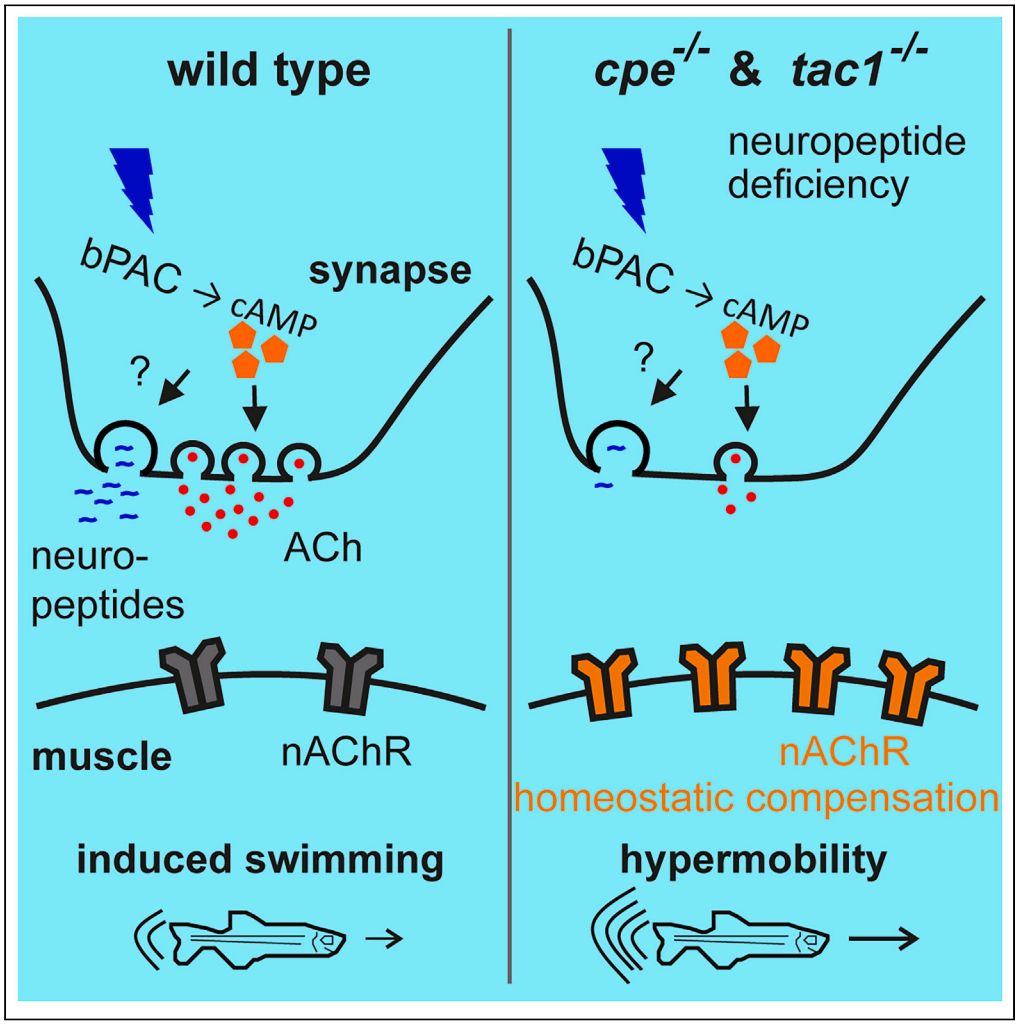

Holger Dill, Jana F. Liewald, Michelle Becker, Marius Seidenthal, Alexander Gottschalk

dill@biochem.uni-frankfurt.de (H.D.)
a.gottschalk@em.uni-frankfurt.de (A.G.)

Highlights

Optogenetic cAMP signaling (bPAC) in larval ZF motor neurons increases locomotion

bPAC photostimulation in motor neurons increases the rate of cholinergic mEPCs

Lack of neuropeptides in *cpe*$^{-/-}$ and *tac1*$^{-/-}$ causes reduced motor neuron ACh output

Postsynaptic homeostatic nAChR upscaling restores transmission in *cpe* and *tac1* mutants

Dill et al., iScience *27*, 110687
September 20, 2024
https://doi.org/10.1016/j.isci.2024.110687

iScience

CellPress
OPEN ACCESS

Article

Neuropeptidergic regulation of neuromuscular signaling in larval zebrafish alters swimming behavior and synaptic transmission

Holger Dill,[1,2,*] Jana F. Liewald,[1,2] Michelle Becker,[1,2] Marius Seidenthal,[1,2] and Alexander Gottschalk[1,2,3,*]

SUMMARY

Chemical synaptic transmission is modulated to accommodate different activity levels, thus enabling homeostatic scaling in pre- and postsynaptic compartments. In nematodes, cholinergic neurons use neuropeptide signaling to modulate synaptic vesicle content. To explore if this mechanism is conserved in vertebrates, we studied the involvement of neuropeptides in cholinergic transmission at the neuromuscular junction of larval zebrafish. Optogenetic stimulation by photoactivated adenylyl cyclase evoked locomotion. We generated mutants lacking the neuropeptide-processing enzyme carboxypeptidase E (*cpe*), and the most abundant neuropeptide precursor in motor neurons, tachykinin (*tac1*). Both mutants showed exaggerated locomotion after photostimulation. Recording excitatory postsynaptic currents demonstrated overall larger amplitudes in the wild type. Exaggerated locomotion in the mutants thus reflected upscaling of postsynaptic excitability. Both mutant muscles expressed more nicotinic acetylcholine receptors (nAChRs) on their surface; thus, neuropeptide signaling regulates synaptic transmitter output in zebrafish motor neurons, and muscle cells homeostatically regulate nAChR surface expression, compensating reduced presynaptic input.

INTRODUCTION

Proper function of the animal nervous system depends on secretion of chemical neurotransmitters such as acetylcholine (ACh) from the presynaptic terminal into the synaptic cleft, and binding of these transmitters to their respective receptors in the postsynaptic compartment. The molecular mechanisms behind this dynamic process and how it is regulated are still not fully understood[1]; however, synaptic efficacy is often controlled by neuromodulators.[2,3] Neurotransmitters are stored in small organelles termed synaptic vesicles (SVs) from which they are released by the neuron through exocytosis. Fusion of SVs with the plasma membrane at the active zone of the synapse is triggered by depolarization and the resulting increase in Ca^{2+} concentration. SV exocytosis is promoted in response to intracellular signaling via cyclic adenosine monophosphate (cAMP) and protein kinase A (PKA) signaling, mediated by diverse synaptic PKA targets that induce SV mobilization and SV priming, such that increases in Ca^{2+} concentration have a higher chance of triggering SV fusion events.[4] Some known PKA targets are synapsin,[5] tomosyn,[6] Rim1,[7] ryanodine receptor,[8] cysteine string protein,[9] snapin,[10] complexin,[11] and SNAP-25.[12] In general, it is beneficial if synaptic transmission can be modulated, to adapt to the demands of the current situation, or to alter synaptic efficacy in the long term. On the presynaptic side, modulation of transmission can be mediated by altering the response of the presynaptic machinery to changes in the Ca^{2+} concentration, thus altering the rate at which SVs are mobilized from the reserve pool[13] or varying the (quantal) content of neurotransmitter per SV.[14] Furthermore, neuromodulators can affect presynaptic transmission, e.g., by altering the number of SVs being produced.[3] Postsynaptic modes of regulating signal efficacy have also been described, for example, changes in the amount of postsynaptic transmitter receptors and their interaction with scaffolding proteins, membrane resistance, or other modes of excitability, like upregulation of voltage-gated ion channels.[15–17]

Although synaptic architecture varies between cell types and species, the ultrastructure of synapses and the composition of SVs and the "pools" into which they are organized are conserved between invertebrates and vertebrates including zebrafish (*Danio rerio*).[18] Structures at neuromuscular junctions (NMJs), the interface between cholinergic motor neurons and skeletal muscle fibers, have been observed in zebrafish larvae using ultrastructural imaging techniques. As in other organisms, they comprise SVs, dense core vesicles (DCVs) containing neuropeptides, and clathrin-coated vesicles.[19] Like other peptide hormones, neuropeptides, which are stored in, and released from, DCVs, originate from longer precursor proteins, which are packaged into vesicles in the *trans*-Golgi network, that are subsequently acidified. Within the DCV, neuropeptide precursor proteins are converted into small bioactive peptides by pro-protein convertase cleavage, and many, but not all,

[1]Buchmann Institute, Goethe University, Max-von-Laue-Strasse 15, D-60438 Frankfurt, Germany
[2]Institute for Biophysical Chemistry, Goethe University, Max-von-Laue-Strasse 9, D-60438 Frankfurt, Germany
[3]Lead contact
*Correspondence: dill@biochem.uni-frankfurt.de (H.D.), a.gottschalk@em.uni-frankfurt.de (A.G.)
https://doi.org/10.1016/j.isci.2024.110687

bioactive peptides are C-terminal trimmed by carboxypeptidase E (CPE), before being released at synaptic terminals.[20–22] In endocrine cells, CPE appears as two isoforms. Full-length CPE associates with membranes in a pH-dependent manner, while a C-terminally truncated, yet enzymatically more active, soluble form is found in the vesicular lumen.[23–25] Although the enzymatic function of CPE during maturation of most neuropeptides is widely accepted, further roles of CPE during sorting of proteins into the regulated secretory pathway have been suggested and loss of CPE was proposed to lead to missorting of peptides into the constitutive pathway.[26–28]

In zebrafish, remarkably diverse functions have been associated with neuropeptides. For example, the expression levels of parathyroid hormone 2 (*pth2*) were shown to mirror the presence of conspecifics and also the density of the swarm.[29] Furthermore, galanin (*galn*) expression in the brain is essential for the generation of color patterns by self-organization of pigment cells,[30] while tachykinins (*tac*) are broadly expressed in the central nervous system and have a supposed role as neuromodulators.[31,32] In mammals, tachykinins perform diverse roles, as neuromodulators, or as regulators of pain, stress, sensory processing, inflammation, etc.[33] The human Tac1 precursor gives rise to substance P, neurokinin A, and neuropeptides κ and γ. For zebrafish, the consequences of a broad deficit of neuropeptides, as expected for the *cpe* knockout, have not been described as yet.

The development of optogenetic tools has revolutionized the field of neuroscience by enabling researchers to manipulate specific neurons or neuronal populations. Today, optogenetic methods are standard in many model organisms, and thus optogenetic tools to influence neuronal activity have also been established in zebrafish.[34,35] Microbial rhodopsins for de- and hyperpolarization were used to study the function of sensory neurons[36] or central pattern generators[37] as early as day one of embryonic development, allowing to achieve calibrated light-induced currents and behavior in different sets of neurons, among them motor neurons.[34] In addition to light-activatable ion channels and pumps, other optogenetic tools have emerged in recent years. One class of tools for optogenetic manipulation are photoactivated adenylyl cyclases (PACs) such as bPAC, mediating light-dependent synthesis of the second messenger cyclic AMP (cAMP) for precise temporal and spatial control and acute tuning of intracellular cAMP concentrations.[38–41] bPAC was shown to be enzymatically active in early zebrafish embryos[42] and has been applied to analyze the role of cAMP signaling in axonal regeneration or to induce swimming behavior by activating hindbrain reticulospinal V2a neurons.[43]

We have previously analyzed the effects of cAMP generation in presynaptic terminals of cholinergic motor neurons in the nematode *Caenorhabditis elegans*. This uncovered an as yet unknown role of neuropeptides in the regulation of synaptic transmission and plasticity,[14] which, apart from increasing the rate of SV release, also affected the filling state of SVs with ACh. Thus, synaptic transmission can be controlled by two regimes: depolarization and Ca^{2+} concentration control the acute fusion of SVs, while cAMP and peptidergic signaling alter the transmitter content per SV. This way, in addition to network activity of central pattern generators, motor neurons can integrate pathways of neuromodulation in different systemic states.

Expression of bPAC and the consequences of increased synaptic cAMP levels have not been described in zebrafish motor neurons to our knowledge. In this study we explored whether the dual control of neuronal transmission, as described in *C. elegans*,[14] is conserved also in vertebrates, specifically in zebrafish. We expressed bPAC in spinal motor neurons and photostimulated larvae at different developmental stages. This evoked exaggerated, but coordinated, locomotion, as well as increased SV fusion rates and miniature excitatory postsynaptic currents (mEPSCs). We generated deletion alleles of the main neuropeptide-processing enzyme, *cpe*, as well as of the most abundantly expressed neuropeptide in cholinergic motor neurons, *tac1*. Both mutants showed enhanced behavioral effects in response to bPAC stimulation. Likely, this occurred in response to presynaptic defects, like smaller mEPSC amplitude and lower SV release rates, as a consequence of postsynaptic compensation. The latter involves increased expression of nAChRs in the neuromuscular endplates. Thus, mechanisms of cholinergic neuromodulation by neuropeptides appear to exist also in zebrafish, even though the details seem to differ between vertebrates and invertebrates.

RESULTS

Activation of bPAC in cholinergic motor neurons enhances locomotion activity

In order to analyze the effect of ChR2 and bPAC stimulation in embryonic and larval zebrafish motor neurons, we generated transgenic lines expressing the respective optogenetic tools. The *mnx1* promotor[44,45] has been described to be specifically active in primary and secondary motorneurons (PMNs and SMNs, respectively). We took two approaches: (1) we used the *mnx1* promotor fragment to directly express a fusion protein consisting of bPAC and EGFP (*Tg[mnx1En:bPAC-egfp]*); (2) we harnessed the *Tg[mnx1:Gal4]* driver line as a means to express ChR2 and bPAC from the *Tg[UAS:ChR2-P2A-dTomato]* and *Tg[UAS:bPAC-V2A-mCherry]*[42] transgenes, respectively. EGFP and dTomato fluorescence were clearly visible in PMN cell bodies and axons as early as 24 h post fertilization (hpf) (Figure 1A, left panels). Corresponding expression of the ChR2 and bPAC transgenes in PMNs and SMNs could be observed at 4 days post fertilization (dpf) (Figure 1A, right panels).

To test whether cholinergic motor neurons can be activated and neuromuscular signaling increased by elevated cAMP levels, behavioral assays of locomotion phenotypes were used. bPAC enzymatically generates cAMP upon activation by blue light of approximately 441 nm.[40] cAMP signaling, through PKA and its presynaptic targets, is expected to evoke increased neuronal activity, also in zebrafish motor neurons. Similarly, ChR2 depolarizes neurons during stimulation with blue light[46] and is thus expected to evoke motor activity.[35,47,48] Blue light stimulus frequency and intensity were optimized for the application of ChR2 and bPAC in accordance with previous work by others.[34] Motor activity in zebrafish embryos starts around 17 hpf with a side-to-side movement of the tail, a characteristic behavior called spontaneous tail coiling.[49] Since this behavior is mediated by motor neurons and interneurons in the spinal cord and depends on slow muscles,[50] we reasoned that it could be a possible early measure for optogenetically evoked neuromuscular activity as well. Wild-type and transgenic zebrafish embryos at 24 hpf showed a similar baseline coiling rate under dark conditions (Figures 1B and S1A). Blue light stimulation of wild-type animals did not

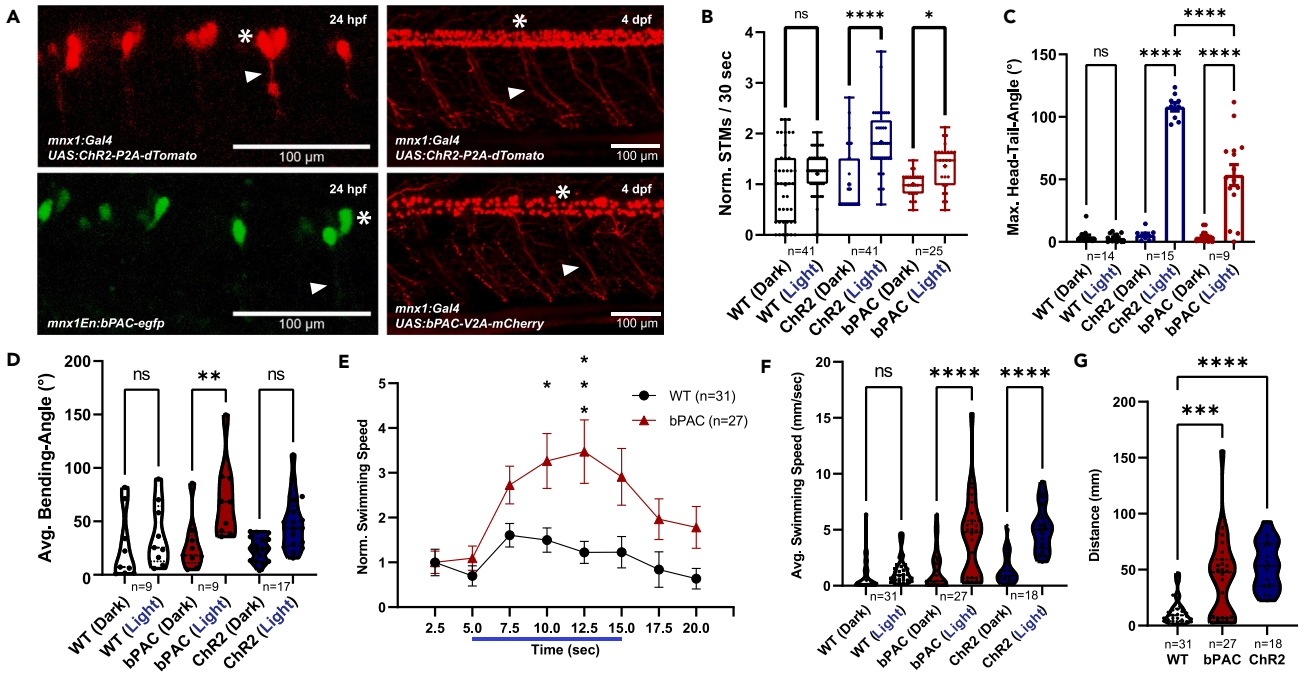

Figure 1. Expression and stimulation of ChR2 and bPAC in zebrafish motor neurons alter locomotion behavior

(A) Confocal images of Tg[*mnx1:Gal4*]/Tg[*UAS:ChR2-P2A-dTomato*] and Tg[*mnx1En:bPAC-egfp*] transgenic embryos (24 hpf) and of Tg[*mnx1:Gal4*]/Tg[*UAS:ChR2-P2A-dTomato*] and Tg[*mnx1:Gal4*]/Tg[*UAS:bPAC-V2A-mCherry*] double transgenic larvae (4 dpf). Asterisks mark motor neuron cell bodies, arrowheads motor axons.

(B) Spontaneous (dark) and evoked (light) tail movements (STMs/ETMs) in 24 hpf embryos.

(C) Head-tail angles in immobilized larvae under dark and blue-light conditions. The maximum head-tail angles were determined for wild-type (WT), bPAC (Tg[*mnx1: Gal4*]/Tg[*UAS: bPAC-V2A-mCherry*]), and ChR2 (Tg[*mnx1:Gal4*]/Tg[*UAS:ChR2-P2A-dTomato*] transgenic larvae (4 dpf).

(D) Bending angles of freely swimming larvae under dark and photostimulated conditions. The bending angles were determined for animals as in (C).

(E) Swimming speed was measured for individuals 4 dpf before, during, and after blue light stimulation.

(F) Average swimming speed with and without blue light stimulation.

(G) Distance traveled during the photostimulation phase. In (B), median (cross), 25/75 quartiles, and min to max are shown; in (C) and (E), means ± SEM; in (D) and (F and G), median and 25/75 quartiles (thick and thin black lines), min to max are shown. in (B), Kruskal-Wallis test with Dunn *post hoc* test.; in (C–F), two-way ANOVA; in (G), one-way ANOVA, each with Tukey multiple comparisons of means. Statistical significance given as ****$p < 0.0001$, ***$p < 0.001$, **$p < 0.01$, *$p < 0.05$.

See also Figure S1.

evoke significant changes in behavior; however, for both, ChR2 or bPAC, blue light induced a significantly increased coiling rate in transgenic embryos, as compared to the respective condition without stimulus (Figures 1B and S1A; Videos S1, S2, and S3).

To analyze if activation of bPAC and, consequently, the increase of cAMP levels or the stimulation of ChR2 in motor neurons also trigger any locomotion changes in older zebrafish larvae, we performed further assays. Observing induced locomotion in partially immobilized larvae is an established way to determine if a certain input triggers, e.g., an escape response or augmented swimming attempts.[35,51] To this end, we measured the maximum deviation of the tail tip from the body axis, namely the angle between head and tail, in 4 dpf head-mounted animals, in the dark, and following blue light stimulation. Whole-field illumination and respective activation of bPAC and ChR2 in all motor neurons led to large amplitude tail bends (Figure 1C; Videos S4, S5, and S6), while wild-type larvae did not exhibit any change in behavior and no escape responses. This indicates that bPAC as well as ChR2 can specifically activate MNs. We did not observe any seizure- or paralysis-like behavior in this assay. This indicates that MN activity was not induced by massive depolarization but, rather, that their membrane potential was elevated, such that intrinsic circuit activity evoked behavior more readily, yet in a coordinated way, to trigger muscle contraction. Based on the deeper bending angles, contractions were more pronounced for ChR2 stimulation.

Strong tail beating as evoked by MN stimulation via bPAC or ChR2 in immobilized larvae is expected to lead to an increased swimming speed in freely behaving animals. In contrast to the coiling behavior described earlier, burst swimming in older larvae is executed mainly by fast muscles upon coordinated input from MNs.[50] We established a method to record swimming behavior and quantify swimming parameters like the body bending angle and speed of larval zebrafish over time. Individual larvae (4 dpf) were placed in an agarose arena and subjected to an illumination protocol as described in STAR Methods. Wild-type larvae exhibit a mild escape response upon illumination with bright blue light, as described previously.[52] However, a significantly stronger response was observed in bPAC and ChR2 transgenic larvae (Tg[mnx1:Gal4]/Tg[UAS:bPAC-V2A-mCherry], Tg[mnx1:Gal4]/Tg[UAS:ChR2-P2A-dTomato]) (Video S7). This became evident as increases

in bending angles (Figure 1D), swimming speed during the blue light stimulation phase (Figures 1E, 1F, and S1B–S1D), and the distance which larvae cover during light stimulation (Figure 1G). Particularly bPAC-expressing animals showed a significant increase in locomotion behavior as compared to non-transgenic wild-type animals. Yet, some bPAC transgenic larvae did not respond to the blue light stimulus (Figures 1F and 1G). Since we did not observe this for ChR2 transgenics (Figures 1F and 1G), we speculated that this might be due to dark activity of bPAC,[39] and adaptation of cAMP pathways.

Our findings in behavioral assays demonstrate that ChR2-induced depolarization of cholinergic motor neurons causes rapid behavioral changes (e.g., tail beating and swimming) which originate from enhanced activity of slow or fast muscles, respectively.[50] bPAC stimulation evokes similar effects. These findings are in line with the hypothesis that an increased cAMP level in cholinergic cells might lead to increased rates of SV fusion and exocytosis of the neurotransmitter ACh.

Neuropeptide signaling genes are expressed in larval motor neurons

We found that optogenetic cAMP generation induced locomotion behavior. Similar observations were made in motor neurons of other organisms. These could be linked to neuromodulatory activity, specifically signaling via neuropeptides, which in *C. elegans* was found to regulate the filling state of cholinergic SVs.[14] Previous studies revealed that cholinergic neurons in zebrafish express neuropeptides[53] and larval motor neurons contain DCVs, as visualized by electron microscopy.[19] However, it is not firmly established which roles these neuropeptides have. Given the cAMP effects on locomotion, we wondered if some of these neuropeptides might be involved in modulation of signal transmission at NMJs in zebrafish. Therefore, we analyzed whether key components of the neuropeptide machinery are expressed in motor neurons. Similar to other vertebrates, zebrafish neuropeptides are derived from longer precursor proteins, which undergo enzymatic post-translational processing in DCVs.[21] Publicly available single-cell RNA sequencing data[54] and RNA *in situ* hybridization showed that *cpe*, which is involved in biosynthesis of most (but not all) neuropeptides and peptide hormones,[20,55,56] is expressed in spinal cord neurons and motor neurons of 24 hpf embryos and 4 dpf zebrafish larvae, respectively (Figures 2A and S2). By mass spectrometry analysis of whole brain lysates, 62 neuropeptides originating from 34 different peptide precursors were identified in zebrafish,[57] and expression of several neuropeptides, likely in the central nervous system, was validated. Furthermore, expression profiling of zebrafish neurons at 4 dpf by single-cell RNA sequencing[54] identified a particular cluster of mRNA profiles (cluster #143) containing prominent marker genes for motor neurons like *mnx1* and *isl1* (Figure S2). The same cell cluster expresses the neuropeptide precursor tachykinin 1 (*tac1*) at high level and with high significance in comparison to the entire cell atlas (Figure S2). Likewise, 24 hpf embryos exhibited strong expression of *tac1* mRNA in the brain and in a region of the spinal cord anatomically known to contain motor neurons (Figure 2A). These data suggest that certain neuropeptides are expressed and processed into their active form in, and are likely also released from, motor neurons during developmental stages relevant for our analysis. Hence, in the following experiments, we focused on the candidate genes *cpe* and *tac1*.

Knockout of *cpe* and *tac1* by CRISPR-mediated gene deletion

To obtain knockouts, we used CRISPR-Cas9 technology, employing two single guide RNAs (sgRNAs) for each target gene (Figure 2B). For *cpe*, the resulting 277 bp deletion affects part of the 5′-UTR, the start codon, and 202 bp of the coding sequence. For the *tac1* gene, we could induce a 564 bp deletion including part of the promotor, transcriptional start site, 5′-UTR, start codon, and the first 114 bp of the coding sequence together with the first splice site and a part of the first intron. This ultimately leads to a *tac1* mRNA retaining part of the first intron (Figure S2E), which even if it were translated, should have numerous frameshifts and premature stop codons. Furthermore, in both the *cpe Δ277* and *tac1 Δ564* alleles, the respective mutant mRNA levels were significantly reduced as compared to wild type animals (Figures 2C, 2D, and S2D). Together, these findings strongly suggest a loss of the respective precursor proteins as well. Due to genetic compensation events, paralogues of mutated genes are frequently upregulated.[58,59] To survey if this is also the case for the tachykinin gene family, we performed quantitative PCR analysis of *tac3a*, *tac3b*, and *tac4* expression in the *tac1* mutant background. We did not observe any upregulation of other tachykinin family members in $tac1^{-/-}$ animals (Figure S2D). $cpe^{-/-}$ and $tac1^{-/-}$ knockout larvae had no obvious morphological phenotype and developed normally until 4 dpf. Moreover, frequencies of genotypes observed from heterozygous breedings approximately matched the expected Mendelian inheritance patterns in 4 dpf larvae (Figure 2E). Although $cpe^{-/-}$ homozygous mutants develop normally until 4 dpf (Figure S2F), they exhibit low survival rates during later development and die during juvenile stages, while $tac1^{-/-}$ knockout animals develop to adults without obvious phenotypes. Hence, *cpe* and *tac1* homozygous knockout animals, as described earlier, were used for further experiments to analyze whether neuropeptides play a role in the cAMP-induced locomotion phenotype observed in photostimulated bPAC transgenic animals.

Neuropeptides modulate signal transmission at zebrafish NMJs

We subjected $cpe^{-/-}$ and $tac1^{-/-}$ animals to a swimming assay before and during bPAC stimulation, as described earlier. Basal locomotion speed during swimming before blue light stimulation was similar between wild-type animals as well as bPAC transgenic wild-type and homozygous $cpe^{-/-}$ or $tac1^{-/-}$ siblings (Figures S3A and S3B; Video S7). When photostimulated, we found that homozygous *cpe* mutants swam significantly faster as compared to their wild-type and heterozygous siblings. We could not observe significant differences in swimming behavior of $cpe^{+/+}$ and $cpe^{+/-}$ siblings under bPAC stimulation (Figures 3A, S3C, and S3D). A similar effect was evident in *tac1* knockouts, though less pronounced (Figure 3B). These findings could indicate that neuropeptides have a negative contribution to neuromuscular signaling, and thus, in their absence, higher locomotion speed increases are observed. Alternatively, neuropeptide signaling may positively influence synaptic transmission, and the observed increase of the behavioral response could be due to postsynaptic homeostatic scaling,

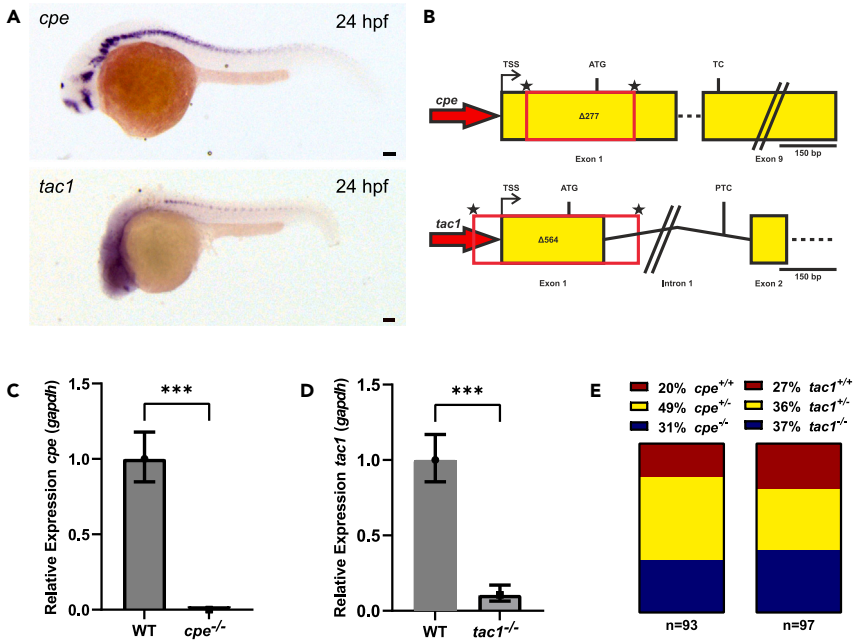

Figure 2. Key components of the neuropeptide signaling pathway are expressed in motor neurons

(A) Bright-field images of *in situ* hybridization stainings for *cpe* and *tac1* mRNAs, respectively. Scale bars, 100 μm.

(B) Schematic representation of *cpe* and *tac1* gene loci illustrating the CRISPR-Cas9 knockout strategy. Asterisks indicate sgRNA target sites. TSS, transcriptional start site; ATG, start codon; TC, termination codon; PTC, premature termination codon.

(C) qPCR showing *cpe* mRNA levels relative to *gapdh*.

(D) qPCR showing *tac1* mRNA levels relative to *gapdh*.

(E) Percentage of wild-type, heterozygous, and homozygous genotypes within a population of 4 dpf *cpe* or *tac1* mutant larvae. In (C) and (D), means ± SEM are shown; Student's t test. Statistical significance given as ***$p < 0.001$.

See also Figure S2.

compensating for a presynaptic deficit. *tac1* could encode one of the neuropeptides responsible for the observed phenotypes but is not solely responsible for the effects as observed in the *cpe* knockout animals.

Patch-clamp recording from muscle cells shows altered transmission in $cpe^{-/-}$ and $tac1^{-/-}$ mutants following bPAC photostimulation of MNs

To further characterize the mutants, and to explore the possible cause for their altered locomotion, we turned to electrophysiology. Homozygous mutant animals were chosen for further analysis after genotyping on day 2 of development. We recorded from the superficial ("slow")

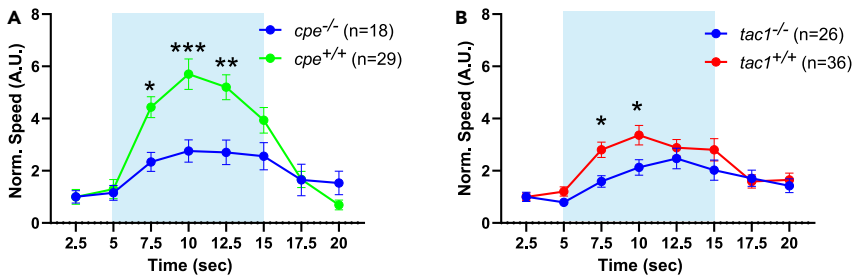

Figure 3. Enhanced locomotion behavior during bPAC stimulation in *cpe* and *tac1* knockouts

(A) *cpe* homozygous knockouts and wild-type siblings (4 dpf) in the Tg[*mnx1:Gal4*]/Tg[*UAS:bPAC-V2A-mCherry*] double transgenic background were subjected to a swimming assay and swimming speed measured during blue light stimulation as indicated. Values are normalized to the first 2.5 s before illumination. Two-way ANOVA with Tukey multiple comparisons of means.

(B) Swimming speed of *tac1* homozygous knockouts and respective wild-type siblings (4 dpf) carrying the Tg[*mnx1:Gal4*]/Tg[*UAS:bPAC-V2A-mCherry*] transgenes before, during, and after bPAC activation. Values are normalized to the first 2.5 s before illumination. Two-way ANOVA with Tukey multiple comparisons of means. Data are displayed as means ± SEM. Statistical significance given as ***$p < 0.001$, **$p < 0.01$, *$p < 0.05$.

See also Figure S3.

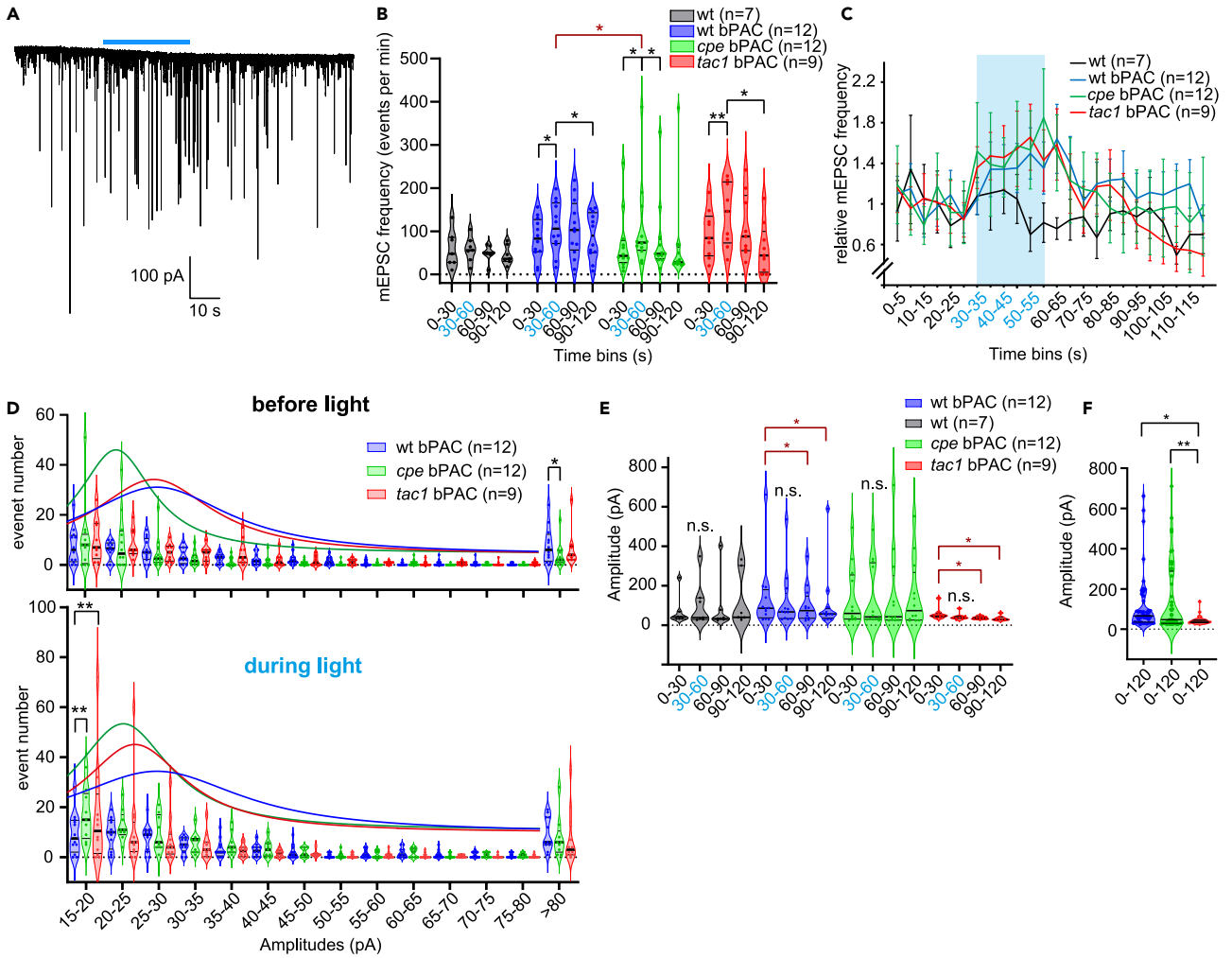

Figure 4. Post-synaptic recording from the NMJ following bPAC photostimulation demonstrates altered signaling in *cpe* and *tac1* knockout animals

(A) Representative recording of mEPSCs before, during, and after bPAC photostimulation (blue bar) in a wild-type animal expressing bPAC in cholinergic motor neurons.

(B) mEPSC frequencies were analyzed in different time bins, as indicated, in wild-type animals, as well as in bPAC-expressing animals, either wild-type siblings or $cpe^{-/-}$ or $tac1^{-/-}$ knockout animals.

(C) Normalized mEPSC rates analyzed in 5 s time bins, as indicated, in the respective animals as in (B). Blue shade indicates time of blue light exposure. Data are displayed as means ± SEM.

(D) Number of mEPSC events of a given amplitude interval, as indicated, observed over a 30 s interval before photostimulation (upper panel) or during the photostimulation (lower panel), for animals expressing bPAC, in wild-type, or $cpe^{-/-}$ or $tac1^{-/-}$ knockout animals.

(E) mEPSC amplitudes were analyzed for each strain in 30 s intervals as indicated, before, during, and after photostimulation.

(F) All mEPSC amplitudes across all intervals were analyzed for bPAC-expressing animals (wild type, or $cpe^{-/-}$ or $tac1^{-/-}$ knockouts, as indicated). In (B) and (D–F), median and 25/75 quartiles (thick and thin black lines), min to max are shown. Two-way ANOVA, Tukey test. In (B) and (E), red significance labels analyses using Fisher Test. Statistical significance given as $^{**}p < 0.01$, $^{*}p < 0.05$; n.s., non-significant.

muscles,[50] which are innervated by the secondary motor neurons[60] of dissected larvae at 4 dpf, in voltage-clamp mode, before, during, and after 30 s blue light stimulation of cholinergic neurons expressing bPAC (Figure 4A). During these experiments we found that a certain fraction of wild-type animals did not show any effect during light stimulation in patch-clamp recordings, even though expressing bPAC protein and responding to stimulation by a swimming response (judged by visual inspection; here we could not quantify this due to time constraints; note that we observed non-responders also in behavioral experiments; Figures 1F and 1G). This might be due to the damage of the innervating MNs during the preparation. Since the number of animals which can be evaluated by electrophysiology is very limited, we excluded the individuals described earlier from statistical analysis. We analyzed the rate of mEPSCs, which are evident as single current spikes of different amplitudes and are believed to reflect single SV fusion events.[61] The basal rates of mEPSCs were smaller in wild-type than in bPAC-expressing animals (Figure 4B), indicating an effect of bPAC expression, likely due to the known dark activity of bPAC, leading to elevated basal cAMP

levels.[40] Also, *cpe*$^{-/-}$ animals expressing bPAC showed a lower basal mEPSC frequency compared to wild-type and *tac1*$^{-/-}$ animals, though not reaching significance. When analyzed over the entire period of the experiment, normalized mEPSC frequency showed a significant increase during the blue light exposure in all bPAC-expressing strains, but not in wild-type non-transgenic animals (Figures 4B and 4C). This increase was significantly smaller in *cpe*$^{-/-}$ animals, indicating a role of neuropeptides in regulating the rate of SV release or, possibly, mobilization. This neuropeptide, however, seems not to be encoded by *tac1*, as there was no difference observed in these mutants.

Next, we analyzed the mEPSC amplitudes (Figures 4D–4F). Amplitudes exhibited a wide range between few dozen pA and up to 700 pA, in rare cases even >1 nA (Figure 4F), as observed previously.[62–64] This is difficult to reconcile, assuming single SV fusion events are causing these high-amplitude mEPSCs. Remarkably high amplitudes could for example be due to different characteristics of release sites that are more or less precisely located opposite of clusters of postsynaptic nAChRs,[60] which mediate the currents underlying mEPSCs; but also simultaneous release of multiple SVs from one site may have to be considered, as well as electrical coupling in the slow muscle ensemble.[62] When we analyzed the mEPSC amplitudes before and during the photostimulation in the different genotypes, a similar distribution of frequencies and amplitudes became apparent (Figure 4D). Before stimulation, *cpe*$^{-/-}$ and *tac*$^{-/-}$ animals showed a trend to smaller mEPSC amplitudes, which was significant during photostimulation, while wild-type animals showed significantly more of the large mEPSC events (>80 pA) compared to *cpe*$^{-/-}$ mutants. When analyzing mean amplitudes in 30 s intervals before, during, and after the light stimulus, there were significantly smaller amplitude events following the light pulse in wild-type and *tac1*$^{-/-}$, but not *cpe*$^{-/-}$, animals (Figure 4E). *tac1*$^{-/-}$ animals, however, showed a significantly more uniform distribution of mEPSC amplitudes throughout, ranging from 20 to 100 pA (Figure 4F).

In sum, the *cpe*$^{-/-}$ mutants, which are generally affected for neuropeptide signaling, showed fewer mEPSC events during photostimulation, more of the small and less of the large amplitude mEPSC events, while *tac1*$^{-/-}$ mutants had generally more uniform mEPSCs of moderate size. These findings may indicate that several neuropeptides with different modulatory effects could be involved in NMJ signaling. One of them may be inhibitory and lead to the reduced amplitudes after photostimulation, while the other could be promoting larger amplitude events; this latter peptide may be tac1, as these larger amplitudes were clearly absent in *tac1*$^{-/-}$ mutants.

cpe$^{-/-}$ and *tac*$^{-/-}$ mutants express more postsynaptic nAChRs, possibly to compensate for altered neuronal ACh signaling

In behavioral experiments, we observed an increased locomotion of *cpe* and *tac1* mutants in response to bPAC photostimulation, while these mutants were defective for presynaptic release of neurotransmitter. This could be explained by the absence of certain inhibitory neuropeptides in these mutants. Alternatively, there may be some homeostatic mechanism effective in the postsynaptic compartment that compensates for the reduced presynaptic cholinergic signal. One possible scenario of how this could be achieved involves reorganization or increased expression of nAChRs on the surface of muscle cells. To probe this hypothesis, we stained nAChRs using fluorescently labeled α-bungarotoxin in 4 dpf larvae, i.e., in the same developmental stage the swimming assays were performed. α-bungarotoxin binds specifically to the α subunit of mature nAChRs; thus the resulting fluorescence signal reflects the amount and distribution of receptors on the muscle cell surface. Commonly, intense staining in large, connected clusters at the boundary regions between myotomes can be observed, representing NMJs of slow muscle (Figures 5A and 5B), as well as nAChRs in small discrete spots, likely representing NMJs innervating fast muscle cells.[65–67] We found that in *cpe* and *tac1* mutants the mean number of small (rectangle in Figure 5B) and large clusters (dashed rectangle in Figure 5B) were not significantly different compared to wild-type animals (Figures S4A and S4B). The size of the small clusters was significantly larger in *cpe*$^{-/-}$ mutants, while the size of the large clusters was not affected by loss of *cpe* or *tac1* (Figures S4C and S4D). However, the fluorescence intensity of the small clusters was significantly increased in the *cpe* and *tac1* mutants (Figure 5C) and strongly increased in large clusters for the *cpe* knockout (Figure 5C). This might indicate that diminished cholinergic output from motor neurons, due to a loss of neuropeptides, is postsynaptically compensated by localizing more nAChRs to the muscle surface.

DISCUSSION

The function of the NMJ is to excite muscle ensembles in a coordinated manner, enabling movement of body parts, or for general locomotion. Different types of locomotion, i.e., slow, moderate swimming, or corrections of ongoing drifting movement, vs. rapid and vigorous swimming as part of an escape response, require different amounts of neurotransmitter release. Thus, motor neurons need to be able to secrete ACh in different quantities, which can be affected by different regulatory mechanisms, that are listed in the following. (1) Increasing depolarization causes increased action potential frequency, thus leading to fusion and mobilization of more SVs. (2) The level of SV mobilization and priming can affect overall transmitter release, as more SVs will fuse upon arrival of an action potential. (3) As observed in some species, the amount of released transmitter can also be mediated by the amount of ACh loaded into individual SVs. In the latter case, more release of ACh can be achieved from the same number of SVs, and this can be regulated in a very short time, using already existing SVs, and not requiring *de novo* SV formation at the synaptic endosome. In *C. elegans*, acute loading of SVs with ACh was observed in response to a rise in synaptic cAMP levels, using optogenetic stimulation,[14] and this required the release of neuropeptides from cholinergic motor neurons, thus likely acting in an autocrine fashion to influence the loading of SVs with ACh. In a natural setting, it is conceivable that exogenous signals, or intrinsic states of the animal associated with neuromodulatory signals in the motor nervous system (e.g., alertness and escape responses), may cause the increase in cAMP levels, to quickly upregulate neurotransmitter release in addition to the increase in firing rate. Also, more ACh release could be mediated even if the number of SVs becomes limiting, e.g., during periods of prolonged high activity. Our findings indicate that a similar mechanism may be present in zebrafish.

Neuropeptide signaling in zebrafish embryonal motor neurons was thus far mainly linked to developmental aspects of these cells. By electron microscopy, motor neuron terminals were shown to contain DCVs.[19] Genes required for neuropeptide biogenesis, like *cpe*, as well as

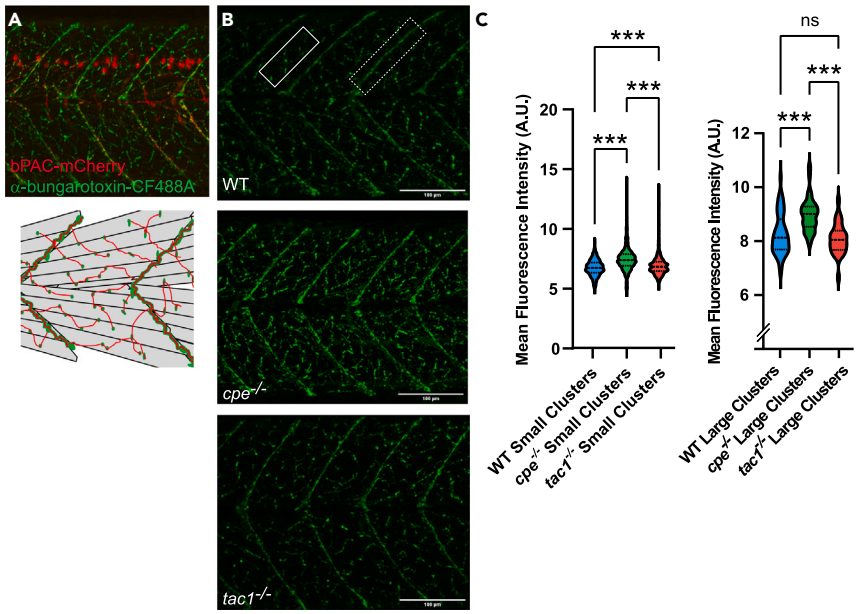

Figure 5. Abundance of nAChRs on muscle cells is altered in neuropeptide mutants

(A) Representative α-bungarotoxin staining at 4 dpf (upper panel). nAChR clusters in green, bPAC-expressing motor neurons in red. Diagram of skeletal muscle cells and clusters of nAChRs on the cell surface (lower panel). Large receptor clusters are assembled on somite boundaries; small receptor clusters are distributed in between.

(B) α-bungarotoxin staining at 4 dpf on wild-type, *cpe*$^{-/-}$, and *tac1*$^{-/-}$ animals. The rectangle in the upper panel represents an area containing small receptor clusters on fast muscle; the dashed rectangle marks larger clusters at the end of slow muscle cells.

(C) Quantification of fluorescence intensity of small and large receptor clusters in the respective zebrafish strains. Median and 25/75 quartiles (thick and thin black lines), min to max are shown. Scale bars in (B): 100 μm. One-way ANOVA with Tukey multiple comparisons of means. Statistical significance given as ***$p < 0.001$; n.s., non-significant.

See also Figure S4.

neuropeptide-encoding genes, have been identified in single-cell RNA sequencing analyses of embryonal cells, clustering along with markers of motor neurons.[54] We showed that two of these genes, *cpe* and *tac1*, are expressed in the spinal cord motor neurons, generated knockouts, and analyzed behavioral and electrophysiological phenotypes, at basal level, and in response to optogenetic stimulation of the MNs using bPAC.

Upon photostimulation, wild-type animals showed a robust behavioral response. In both mutants, *tac1*, and particularly, *cpe*, even higher swimming speed was observed, indicating not a reduction, but rather a gain-of-function of MNs. Alternatively, (postsynaptic) compensation could affect larger increases in swimming speed following bPAC-induced neurotransmitter release. CPE is a central component of the neuropeptide processing machinery in mice,[55] and the observed lethality of juvenile *cpe*$^{-/-}$ zebrafish, though we do not know the exact cause of death, emphasizes this previous finding. Nevertheless, there has been substantial debate about the precise function of CPE in the secretory pathway, including a role as sorting receptor.[20,28] In that context, our result that locomotion behavior of *cpe* wild-type and heterozygous siblings is very similar points to a rather enzymatic, not rate-limiting, role of CPE. This is consistent with recent findings showing that *cpe* heterozygous mice, with reduced *cpe* expression and enzymatic activity, do not have a behavioral phenotype and exhibit wild-type-like quantities of mature neuropeptides.[68]

Our electrophysiological recordings showed that bPAC activation induced an increased rate of mEPSCs. Even though the effect of bPAC stimulation on mEPSC frequency was pronounced, we did observe a large variation in mEPSC amplitudes in slow muscle cells, impeding conclusions as to whether the SV filling state may be altered (increased in response to cAMP signaling in the wild type, lower due to the absence of neuropeptides). Highly variable mEPSC amplitudes have been observed previously in slow muscle, downstream of secondary MNs.[62–64] By bungarotoxin staining and subsequent histological analysis, we observed an increase of large nAChR clusters on slow muscles, in absence of CPE, but only minor effects as in electrophysiological measurements. This may exactly be the outcome of postsynaptic homeostatic upscaling: Lower ACh release due to less SV content is counterbalanced by more postsynaptic nAChRs, in sum leading to similar postsynaptic currents. In the mutants, higher frequency of release (upon bPAC stimulation), meets increased nAChR density, which may lead to increased swimming. The fact that we did not see higher amplitudes in response to bPAC stimulation despite increased behavior may be explained by the involvement of fast muscles, from which we could not measure.

One possible effect of neuropeptide signaling was indicated when we analyzed the mEPSCs in a time-dependent manner. Both wild-type and *tac1* mutants showed smaller mEPSC amplitudes following bPAC photostimulation, which was not observed for *cpe* mutants. While we do not know if some adaptation or fatigue occurred that could explain these reduced amplitudes, the fact that they do not appear in a mutant

(*cpe*) indicates that a neuropeptidergic regulatory mechanism may be involved. A recent study analyzing the prohormone processing in pancreatic β-cells of βCpeKO mice revealed that lack of CPE leads to a decrease of mature peptides, but also an unexpectedly high level of correctly processed (canonical) CPE targets and even upregulation of some incompletely processed proteoforms in *cpe* knockout cells.[69] These findings suggest removal of basic residues by an alternative or compensatory mechanism possibly involving carboxypeptidase D (CPD) and an indirect impact of loss of CPE and its targets on some, otherwise unrelated, peptides. It is unclear how exactly the loss of CPE activity affects the neuropeptidome of zebrafish motor neurons; yet, it can be anticipated that it results in complex changes in the neuropeptide pathway and a reduction in levels of a substantial fraction of neuropeptides. Since the motor neurons express several neuropeptides, there may be a balance of excitatory and inhibitory species that is shifted toward the inhibitory side in the wild type, and not in place in the *cpe* mutant (i.e., no alteration in signaling occurs); in *tac1* mutants, the putative inhibitory signaling is still present, suggesting that *tac1* is not encoding this signal.

In sum, we showed that neuropeptidergic acute signaling occurs at the NMJ of larval zebrafish or that neuropeptides shape NMJ signaling such that acute stimulation via cAMP causes different postsynaptic effects and exaggerated behavior. Whether cAMP triggers neuropeptide release acutely will have to be determined in the future, possibly using fluorescent neuropeptide release reporters to image release events *in vivo* and in real time. However, such reporters have not yet been developed for zebrafish.

Limitations of the study

The current work describes the phenotype of zebrafish larvae whose cholinergic MNs are stimulated by acute optogenetic cAMP generation. This causes enhanced transmitter release, but the study does not provide an answer how exactly cAMP evokes these effects. The two zebrafish mutants generated here for the first time show enhanced behavioral responses to cAMP, while somewhat lower amplitude events were observed that were compensated by higher nAChR densities; yet, the study does not strictly provide a molecular mechanism, how and why. Lower synaptic transmission is opposed by increased postsynaptic nAChR levels, suggesting homeostatic upscaling to underlie these phenotypes; however, the study cannot exclude that developmental aspects altered the mutant NMJs, thus causing phenotypes in a manner non-specific to synaptic transmission. Furthermore, it was shown previously that CPE is required for processing of most but not all prohormones and neuropeptide precursors,[69] thus some compensatory neuropeptide may be counteracting the loss of others. Zebrafish MNs express other, and maybe as yet unknown, neuropeptides, which might have similar abundance in WT and $cpe^{-/-}$ larvae. Last, bPAC has some dark activity,[39] thus the neurons may have altered their activity levels in response to these low, but presumably more than native, levels of cAMP.

STAR★METHODS

Detailed methods are provided in the online version of this paper and include the following:

- KEY RESOURCES TABLE
- RESOURCE AVAILABILITY
  - Lead contact
  - Materials availability
  - Data and code availability
- EXPERIMENTAL MODEL AND STUDY PARTICIPANT DETAILS
  - Zebrafish maintenance and breeding
- METHODS DETAILS
  - Molecular biology
  - Whole mount *in situ* hybridization
  - Microinjection of zebrafish embryos
  - Genotyping of adult zebrafish
  - Genotyping of live zebrafish embryos
  - RT-PCR
  - Quantitative RT-PCR
  - α-Bungarotoxin staining
  - Confocal laser scanning microscopy and image analysis
  - Bright-field microscopy
  - Zebrafish behavioral assays
  - Evoked tail-coiling
  - Tail-beat-assay with immobilized larvae
  - Swimming assay
  - Analysis of head-tail angles in freely behaving larvae
  - Electrophysiology
- QUANTIFICATION AND STATISTICAL ANALYSIS

SUPPLEMENTAL INFORMATION

Supplemental information can be found online at https://doi.org/10.1016/j.isci.2024.110687.

ACKNOWLEDGMENTS

We are grateful to Dr. Soojin Ryu (Johannes Gutenberg-Universität Mainz, Mainz) for the ChR2-P2A-dTomato plasmid, and to Dr. Hernán Lopez-Schier and Dr. Amparo Acker-Palmer for the zebrafish lines. We thank Franziska Baumbach, Hans-Werner Müller, and Katharina Kuhlmeier for expert technical assistance and laboratory management. We acknowledge the animal caretakers at the Goethe-University Biologicum, Ema Omeragić and Deeksha Gopinath Krishnamoorthy for help with animal husbandry, and Dr. Bettina Kirchmaier for assistance with approval procedures. This work was supported by Deutsche Forschungsgemeinschaft grant GO1011/19-1 and CRC1080-B02, to A.G., and by funds from Goethe University.

AUTHOR CONTRIBUTIONS

Conceptualization: H.D. and A.G. Methodology: H.D., J.F.L., and A.G. Software: H.D. and M.S. Validation: H.D., J.F.L., and A.G. Formal analysis: H.D. and A.G. Investigation: H.D., J.F.L., M.B., and A.G. Resources: H.D., J.F.L., M.S., and A.G. Data curation: H.D., J.F.L., and A.G. Writing – original draft: H.D., J.F.L., and A.G. Writing – review and editing: H.D., J.F.L., and A.G. Visualization: H.D. and A.G. Supervision: A.G. Project administration: A.G. Funding acquisition: A.G.

DECLARATION OF INTERESTS

The authors declare no competing interests.

Received: January 11, 2024
Revised: April 13, 2024
Accepted: August 5, 2024
Published: August 6, 2024

REFERENCES

1. Südhof, T.C. (2013). Neurotransmitter release: the last millisecond in the life of a synaptic vesicle. Neuron *80*, 675–690. https://doi.org/10.1016/j.neuron.2013.10.022.
2. Civelli, O. (2012). Orphan GPCRs and neuromodulation. Neuron *76*, 12–21. https://doi.org/10.1016/j.neuron.2012.09.009.
3. Patzke, C., Brockmann, M.M., Dai, J., Gan, K.J., Grauel, M.K., Fenske, P., Liu, Y., Acuna, C., Rosenmund, C., and Südhof, T.C. (2019). Neuromodulator Signaling Bidirectionally Controls Vesicle Numbers in Human Synapses. Cell *179*, 498–513.e22. https://doi.org/10.1016/j.cell.2019.09.011.
4. Maximov, A., Shin, O.H., Liu, X., and Südhof, T.C. (2007). Synaptotagmin-12, a synaptic vesicle phosphoprotein that modulates spontaneous neurotransmitter release. J. Cell Biol. *176*, 113–124. https://doi.org/10.1083/jcb.200607021.
5. Hosaka, M., Hammer, R.E., and Südhof, T.C. (1999). A phospho-switch controls the dynamic association of synapsins with synaptic vesicles. Neuron *24*, 377–387.
6. Gracheva, E.O., Burdina, A.O., Holgado, A.M., Berthelot-Grosjean, M., Ackley, B.D., Hadwiger, G., Nonet, M.L., Weimer, R.M., and Richmond, J.E. (2006). Tomosyn inhibits synaptic vesicle priming in Caenorhabditis elegans. PLoS Biol. *4*, e261. https://doi.org/10.1371/journal.pbio.0040261.
7. Lonart, G., Schoch, S., Kaeser, P.S., Larkin, C.J., Südhof, T.C., and Linden, D.J. (2003). Phosphorylation of RIM1alpha by PKA triggers presynaptic long-term potentiation at cerebellar parallel fiber synapses. Cell *115*, 49–60.
8. Rodriguez, P., Bhogal, M.S., and Colyer, J. (2003). Stoichiometric phosphorylation of cardiac ryanodine receptor on serine 2809 by calmodulin-dependent kinase II and protein kinase A. J. Biol. Chem. *278*, 38593–38600. https://doi.org/10.1074/jbc.C301180200.
9. Evans, G.J., Wilkinson, M.C., Graham, M.E., Turner, K.M., Chamberlain, L.H., Burgoyne, R.D., and Morgan, A. (2001). Phosphorylation of cysteine string protein by protein kinase A. Implications for the modulation of exocytosis. J. Biol. Chem. *276*, 47877–47885. https://doi.org/10.1074/jbc.M108186200.
10. Thakur, P., Stevens, D.R., Sheng, Z.H., and Rettig, J. (2004). Effects of PKA-mediated phosphorylation of Snapin on synaptic transmission in cultured hippocampal neurons. J. Neurosci. *24*, 6476–6481. https://doi.org/10.1523/JNEUROSCI.0590-04.2004.
11. Cho, R.W., Buhl, L.K., Volfson, D., Tran, A., Li, F., Akbergenova, Y., and Littleton, J.T. (2015). Phosphorylation of Complexin by PKA Regulates Activity-Dependent Spontaneous Neurotransmitter Release and Structural Synaptic Plasticity. Neuron *88*, 749–761.
12. Nagy, G., Reim, K., Matti, U., Brose, N., Binz, T., Rettig, J., Neher, E., and Sørensen, J.B. (2004). Regulation of releasable vesicle pool sizes by protein kinase A-dependent phosphorylation of SNAP-25. Neuron *41*, 417–429.
13. Fowler, M.W., and Staras, K. (2015). Synaptic vesicle pools: Principles, properties and limitations. Exp. Cell Res. *335*, 150–156. https://doi.org/10.1016/j.yexcr.2015.03.007.
14. Steuer Costa, W., Yu, S.C., Liewald, J.F., and Gottschalk, A. (2017). Fast cAMP Modulation of Neurotransmission via Neuropeptide Signals and Vesicle Loading. Curr. Biol. *27*, 495–507. https://doi.org/10.1016/j.cub.2016.12.055.
15. Diering, G.H., and Huganir, R.L. (2018). The AMPA Receptor Code of Synaptic Plasticity. Neuron *100*, 314–329. https://doi.org/10.1016/j.neuron.2018.10.018.
16. Barberis, A. (2020). Postsynaptic plasticity of GABAergic synapses. Neuropharmacology *169*, 107643. https://doi.org/10.1016/j.neuropharm.2019.05.020.
17. Droogers, W.J., and MacGillavry, H.D. (2023). Plasticity of postsynaptic nanostructure. Mol. Cell. Neurosci. *124*, 103819. https://doi.org/10.1016/j.mcn.2023.103819.
18. Bruckner, J.J., Zhan, H., and O'Connor-Giles, K.M. (2015). Advances in imaging ultrastructure yield new insights into presynaptic biology. Front. Cell. Neurosci. *9*, 196. https://doi.org/10.3389/fncel.2015.00196.
19. Helmprobst, F., Frank, M., and Stigloher, C. (2015). Presynaptic architecture of the larval zebrafish neuromuscular junction. J. Comp. Neurol. *523*, 1984–1997. https://doi.org/10.1002/cne.23775.
20. Ji, L., Wu, H.T., Qin, X.Y., and Lan, R. (2017). Dissecting carboxypeptidase E: properties, functions and pathophysiological roles in disease. Endocr. Connect. *6*, R18–R38. https://doi.org/10.1530/EC-17-0020.
21. Russo, A.F. (2017). Overview of Neuropeptides: Awakening the Senses? Headache *57*, 37–46. https://doi.org/10.1111/head.13084.
22. Kim, T., Gondré-Lewis, M.C., Arnaoutova, I., and Loh, Y.P. (2006). Dense-core secretory granule biogenesis. Physiology *21*, 124–133. https://doi.org/10.1152/physiol.00043.2005.
23. Fricker, L.D. (1988). Activation and membrane binding of carboxypeptidase E. J. Cell. Biochem. *38*, 279–289. https://doi.org/10.1002/jcb.240380407.
24. Fricker, L.D., Das, B., and Angeletti, R.H. (1990). Identification of the pH-dependent

membrane anchor of carboxypeptidase E (EC 3.4.17.10). J. Biol. Chem. *265*, 2476–2482.
25. Dhanvantari, S., Arnaoutova, I., Snell, C.R., Steinbach, P.J., Hammond, K., Caputo, G.A., London, E., and Loh, Y.P. (2002). Carboxypeptidase E, a prohormone sorting receptor, is anchored to secretory granules via a C-terminal transmembrane insertion. Biochemistry *41*, 52–60. https://doi.org/10.1021/bi015698n.
26. Cool, D.R., Normant, E., Shen, F., Chen, H.C., Pannell, L., Zhang, Y., and Loh, Y.P. (1997). Carboxypeptidase E is a regulated secretory pathway sorting receptor: genetic obliteration leads to endocrine disorders in Cpe(fat) mice. Cell *88*, 73–83. https://doi.org/10.1016/s0092-8674(00)81860-7.
27. Cool, D.R., and Loh, Y.P. (1998). Carboxypeptidase E is a sorting receptor for prohormones: binding and kinetic studies. Mol. Cell. Endocrinol. *139*, 7–13. https://doi.org/10.1016/s0303-7207(98)00081-1.
28. Hosaka, M., Watanabe, T., Sakai, Y., Kato, T., and Takeuchi, T. (2005). Interaction between secretogranin III and carboxypeptidase E facilitates prohormone sorting within secretory granules. J. Cell Sci. *118*, 4785–4795. https://doi.org/10.1242/jcs.02608.
29. Anneser, L., Alcantara, I.C., Gemmer, A., Mirkes, K., Ryu, S., and Schuman, E.M. (2020). The neuropeptide Pth2 dynamically senses others via mechanosensation. Nature *588*, 653–657. https://doi.org/10.1038/s41586-020-2988-z.
30. Eskova, A., Frohnhofer, H.G., Nusslein-Volhard, C., and Irion, U. (2020). Galanin Signaling in the Brain Regulates Color Pattern Formation in Zebrafish. Curr. Biol. *30*, 298–303.e293. https://doi.org/10.1016/j.cub.2019.11.033.
31. Ogawa, S., Ramadasan, P.N., Goschorska, M., Anantharajah, A., Ng, K.W., and Parhar, I.S. (2012). Cloning and expression of tachykinins and their association with kisspeptins in the brains of zebrafish. J. Comp. Neurol. *520*, 2991–3012. https://doi.org/10.1002/cne.23103.
32. Zhou, W., Li, S., Liu, Y., Qi, X., Chen, H., Cheng, C.H.K., Liu, X., Zhang, Y., and Lin, H. (2012). The evolution of tachykinin/tachykinin receptor (TAC/TACR) in vertebrates and molecular identification of the TAC3/TACR3 system in zebrafish (Danio rerio). Mol. Cell. Endocrinol. *361*, 202–212. https://doi.org/10.1016/j.mce.2012.04.007.
33. Nässel, D.R., Zandawala, M., Kawada, T., and Satake, H. (2019). Tachykinins: Neuropeptides That Are Ancient, Diverse, Widespread and Functionally Pleiotropic. Front. Neurosci. *13*, 1262. https://doi.org/10.3389/fnins.2019.01262.
34. Antinucci, P., Dumitrescu, A., Deleuze, C., Morley, H.J., Leung, K., Hagley, T., Kubo, F., Baier, H., Bianco, I.H., and Wyart, C. (2020). A calibrated optogenetic toolbox of stable zebrafish opsin lines. Elife *9*, e54937. https://doi.org/10.7554/eLife.54937.
35. Douglass, A.D., Kraves, S., Deisseroth, K., Schier, A.F., and Engert, F. (2008). Escape behavior elicited by single, channelrhodopsin-2-evoked spikes in zebrafish somatosensory neurons. Curr. Biol. *18*, 1133–1137.
36. Portugues, R., Severi, K.E., Wyart, C., and Ahrens, M.B. (2013). Optogenetics in a transparent animal: circuit function in the larval zebrafish. Curr. Opin. Neurobiol. *23*, 119–126. https://doi.org/10.1016/j.conb.2012.11.001.
37. Wyart, C., Del Bene, F., Warp, E., Scott, E.K., Trauner, D., Baier, H., and Isacoff, E.Y. (2009). Optogenetic dissection of a behavioural module in the vertebrate spinal cord. Nature *461*, 407–410. https://doi.org/10.1038/nature08323.
38. Schröder-Lang, S., Schwarzel, M., Seifert, R., Strunker, T., Kateriya, S., Looser, J., Watanabe, M., Kaupp, U.B., Hegemann, P., and Nagel, G. (2007). Fast manipulation of cellular cAMP level by light in vivo. Nat. Methods *4*, 39–42.
39. Ryu, M.H., Moskvin, O.V., Siltberg-Liberles, J., and Gomelsky, M. (2010). Natural and engineered photoactivated nucleotidyl cyclases for optogenetic applications. J. Biol. Chem. *285*, 41501–41508.
40. Stierl, M., Stumpf, P., Udwari, D., Gueta, R., Hagedorn, R., Losi, A., Gärtner, W., Petereit, L., Efetova, M., Schwarzel, M., et al. (2011). Light modulation of cellular cAMP by a small bacterial photoactivated adenylyl cyclase, bPAC, of the soil bacterium Beggiatoa. J. Biol. Chem. *286*, 1181–1188. https://doi.org/10.1074/jbc.M110.185496.
41. Oldani, S., Moreno-Velasquez, L., Faiss, L., Stumpf, A., Rosenmund, C., Schmitz, D., and Rost, B.R. (2021). SynaptoPAC, an Optogenetic Tool for Induction of Presynaptic Plasticity. J. Neurochem. *156*, 324–336. https://doi.org/10.1111/jnc.15210.
42. Xiao, Y., Tian, W., and López-Schier, H. (2015). Optogenetic stimulation of neuronal repair. Curr. Biol. *25*, R1068–R1069. https://doi.org/10.1016/j.cub.2015.09.038.
43. Hagio, H., Koyama, W., Hosaka, S., Song, A.D., Narantsatsral, J., Matsuda, K., Shimizu, T., Hososhima, S., Tsunoda, S.P., Kandori, H., and Hibi, M. (2023). Optogenetic manipulation of neuronal and cardiomyocyte functions in zebrafish using microbial rhodopsins and adenylyl cyclases. Elife *12*, e83975. https://doi.org/10.7554/eLife.83975.
44. Zelenchuk, T.A., and Brusés, J.L. (2011). In vivo labeling of zebrafish motor neurons using an mnx1 enhancer and Gal4/UAS. Genesis *49*, 546–554. https://doi.org/10.1002/dvg.20766.
45. Fowler, D.K., Stewart, S., Seredick, S., Eisen, J.S., Stankunas, K., and Washbourne, P. (2016). A MultiSite Gateway Toolkit for Rapid Cloning of Vertebrate Expression Constructs with Diverse Research Applications. PLoS One *11*, e0159277. https://doi.org/10.1371/journal.pone.0159277.
46. Nagel, G., Szellas, T., Huhn, W., Kateriya, S., Adeishvili, N., Berthold, P., Ollig, D., Hegemann, P., and Bamberg, E. (2003). Channelrhodopsin-2, a directly light-gated cation-selective membrane channel. Proc. Natl. Acad. Sci. USA *100*, 13940–13945.
47. Liewald, J.F., Brauner, M., Stephens, G.J., Bouhours, M., Schultheis, C., Zhen, M., and Gottschalk, A. (2008). Optogenetic analysis of synaptic function. Nat. Methods *5*, 895–902.
48. Zhu, P., Narita, Y., Bundschuh, S.T., Fajardo, O., Schärer, Y.P.Z., Chattopadhyaya, B., Bouldoires, E.A., Stepien, A.E., Deisseroth, K., Arber, S., et al. (2009). Optogenetic Dissection of Neuronal Circuits in Zebrafish using Viral Gene Transfer and the Tet System. Front. Neural Circuits *3*, 21. https://doi.org/10.3389/neuro.04.021.2009.
49. Brustein, E., Saint-Amant, L., Buss, R.R., Chong, M., McDearmid, J.R., and Drapeau, P. (2003). Steps during the development of the zebrafish locomotor network. J. Physiol. Paris *97*, 77–86. https://doi.org/10.1016/j.jphysparis.2003.10.009.
50. Naganawa, Y., and Hirata, H. (2011). Developmental transition of touch response from slow muscle-mediated coilings to fast muscle-mediated burst swimming in zebrafish. Dev. Biol. *355*, 194–204. https://doi.org/10.1016/j.ydbio.2011.04.027.
51. Thiele, T.R., Donovan, J.C., and Baier, H. (2014). Descending control of swim posture by a midbrain nucleus in zebrafish. Neuron *83*, 679–691. https://doi.org/10.1016/j.neuron.2014.04.018.
52. De Marco, R.J., Thiemann, T., Groneberg, A.H., Herget, U., and Ryu, S. (2016). Optogenetically enhanced pituitary corticotroph cell activity post-stress onset causes rapid organizing effects on behaviour. Nat. Commun. *7*, 12620. https://doi.org/10.1038/ncomms12620.
53. Quan, F.B., Dubessy, C., Galant, S., Kenigfest, N.B., Djenoune, L., Leprince, J., Wyart, C., Lihrmann, I., and Tostivint, H. (2015). Comparative distribution and in vitro activities of the urotensin II-related peptides URP1 and URP2 in zebrafish: evidence for their colocalization in spinal cerebrospinal fluid-contacting neurons. PLoS One *10*, e0119290. https://doi.org/10.1371/journal.pone.0119290.
54. Farnsworth, D.R., Saunders, L.M., and Miller, A.C. (2020). A single-cell transcriptome atlas for zebrafish development. Dev. Biol. *459*, 100–108. https://doi.org/10.1016/j.ydbio.2019.11.008.
55. Naggert, J.K., Fricker, L.D., Varlamov, O., Nishina, P.M., Rouille, Y., Steiner, D.F., Carroll, R.J., Paigen, B.J., and Leiter, E.H. (1995). Hyperproinsulinaemia in obese fat/fat mice associated with a carboxypeptidase E mutation which reduces enzyme activity. Nat. Genet. *10*, 135–142. https://doi.org/10.1038/ng0695-135.
56. Fricker, L.D. (1988). Carboxypeptidase E. Annu. Rev. Physiol. *50*, 309–321. https://doi.org/10.1146/annurev.ph.50.030188.001521.
57. Van Camp, K.A., Baggerman, G., Blust, R., and Husson, S.J. (2017). Peptidomics of the zebrafish Danio rerio: In search for neuropeptides. J. Proteomics *150*, 290–296. https://doi.org/10.1016/j.jprot.2016.09.015.
58. Rossi, A., Kontarakis, Z., Gerri, C., Nolte, H., Hölper, S., Krüger, M., and Stainier, D.Y.R. (2015). Genetic compensation induced by deleterious mutations but not gene knockdowns. Nature *524*, 230–233. https://doi.org/10.1038/nature14580.
59. El-Brolosy, M.A., Kontarakis, Z., Rossi, A., Kuenne, C., Günther, S., Fukuda, N., Kikhi, K., Boezio, G.L.M., Takacs, C.M., Lai, S.L., et al. (2019). Genetic compensation triggered by mutant mRNA degradation. Nature *568*, 193–197. https://doi.org/10.1038/s41586-019-1064-z.
60. Wang, W.C., and Brehm, P. (2017). A Gradient in Synaptic Strength and Plasticity among Motoneurons Provides a Peripheral Mechanism for Locomotor Control. Curr. Biol. *27*, 415–422. https://doi.org/10.1016/j.cub.2016.12.010.
61. Brehm, P., and Wen, H. (2019). Zebrafish neuromuscular junction: The power of N. Neurosci. Lett. *713*, 134503. https://doi.org/10.1016/j.neulet.2019.134503.
62. Luna, V.M., and Brehm, P. (2006). An electrically coupled network of skeletal muscle in zebrafish distributes synaptic current. J. Gen. Physiol. *128*, 89–102. https://doi.org/10.1085/jgp.200609501.
63. Ono, F., Shcherbatko, A., Higashijima, S.i., Mandel, G., and Brehm, P. (2002). The

Zebrafish motility mutant twitch once reveals new roles for rapsyn in synaptic function. J. Neurosci. *22*, 6491–6498. https://doi.org/10.1523/JNEUROSCI.22-15-06491.2002.

64. Wen, H., and Brehm, P. (2005). Paired motor neuron-muscle recordings in zebrafish test the receptor blockade model for shaping synaptic current. J. Neurosci. *25*, 8104–8111. https://doi.org/10.1523/JNEUROSCI.2611-05.2005.
65. Ono, F., Higashijima, S., Shcherbatko, A., Fetcho, J.R., and Brehm, P. (2001). Paralytic zebrafish lacking acetylcholine receptors fail to localize rapsyn clusters to the synapse. J. Neurosci. *21*, 5439–5448. https://doi.org/10.1523/JNEUROSCI.21-15-05439.2001.
66. Jacobson, S.M., Birkholz, D.A., McNamara, M.L., Bharate, S.B., and George, K.M. (2010). Subacute developmental exposure of zebrafish to the organophosphate pesticide metabolite, chlorpyrifos-oxon, results in defects in Rohon-Beard sensory neuron development. Aquat. Toxicol. *100*, 101–111. https://doi.org/10.1016/j.aquatox.2010.07.015.
67. Zempo, B., Yamamoto, Y., Williams, T., and Ono, F. (2020). Synaptic silencing of fast muscle is compensated by rewired innervation of slow muscle. Sci. Adv. *6*, eaax8382. https://doi.org/10.1126/sciadv.aax8382.
68. Fricker, L.D., Lemos Duarte, M., Jeltyi, A., Lueptow, L., Fakira, A.K., Tashima, A.K., Hochgeschwender, U., Wetsel, W.C., and Devi, L.A. (2022). Mice heterozygous for a null mutation of CPE show reduced expression of carboxypeptidase e mRNA and enzyme activity but normal physiology, behavior, and levels of neuropeptides. Brain Res. *1789*, 147951. https://doi.org/10.1016/j.brainres.2022.147951.
69. Fulcher, J.M., Swensen, A.C., Chen, Y.C., Verchere, C.B., Petyuk, V.A., and Qian, W.J. (2023). Top-Down Proteomics of Mouse Islets With Beta Cell CPE Deletion Reveals Molecular Details in Prohormone Processing. Endocrinology *164*, bqad160. https://doi.org/10.1210/endocr/bqad160.
70. Schindelin, J., Arganda-Carreras, I., Frise, E., Kaynig, V., Longair, M., Pietzsch, T., Preibisch, S., Rueden, C., Saalfeld, S., Schmid, B., et al. (2012). Fiji: an open-source platform for biological-image analysis. Nat. Methods *9*, 676–682. https://doi.org/10.1038/nmeth.2019.
71. Aleström, P., D'Angelo, L., Midtlyng, P.J., Schorderet, D.F., Schulte-Merker, S., Sohm, F., and Warner, S. (2020). Zebrafish: Housing and husbandry recommendations. Lab. Anim. *54*, 213–224. https://doi.org/10.1177/0023677219869037.
72. Kimmel, C.B., Ballard, W.W., Kimmel, S.R., Ullmann, B., and Schilling, T.F. (1995). Stages of embryonic development of the zebrafish. Dev. Dyn. *203*, 253–310. https://doi.org/10.1002/aja.1002030302.
73. Kwan, K.M., Fujimoto, E., Grabher, C., Mangum, B.D., Hardy, M.E., Campbell, D.S., Parant, J.M., Yost, H.J., Kanki, J.P., and Chien, C.B. (2007). The Tol2kit: a multisite gateway-based construction kit for Tol2 transposon transgenesis constructs. Dev. Dyn. *236*, 3088–3099. https://doi.org/10.1002/dvdy.21343.
74. Hwang, W.Y., Fu, Y., Reyon, D., Maeder, M.L., Tsai, S.Q., Sander, J.D., Peterson, R.T., Yeh, J.R.J., and Joung, J.K. (2013). Efficient genome editing in zebrafish using a CRISPR-Cas system. Nat. Biotechnol. *31*, 227–229. https://doi.org/10.1038/nbt.2501.
75. Hauptmann, G., and Gerster, T. (1994). Two-color whole-mount in situ hybridization to vertebrate and Drosophila embryos. Trends Genet. *10*, 266. https://doi.org/10.1016/0168-9525(90)90008-t.
76. Lambert, C.J., Freshner, B.C., Chung, A., Stevenson, T.J., Bowles, D.M., Samuel, R., Gale, B.K., and Bonkowsky, J.L. (2018). An automated system for rapid cellular extraction from live zebrafish embryos and larvae: Development and application to genotyping. PLoS One *13*, e0193180. https://doi.org/10.1371/journal.pone.0193180.
77. Livak, K.J., and Schmittgen, T.D. (2001). Analysis of relative gene expression data using real-time quantitative PCR and the 2(-Delta Delta C(T)) Method. Methods *25*, 402–408. https://doi.org/10.1006/meth.2001.1262.
78. Swierczek, N.A., Giles, A.C., Rankin, C.H., and Kerr, R.A. (2011). High-throughput behavioral analysis in C. elegans. Nat. Methods *8*, 592–598. https://doi.org/10.1038/nmeth.1625.
79. González-Fraga, J., Dipp-Alvarez, V., and Bardullas, U. (2019). Quantification of Spontaneous Tail Movement in Zebrafish Embryos Using a Novel Open-Source MATLAB Application. Zebrafish *16*, 214–216. https://doi.org/10.1089/zeb.2018.1688.
80. Creton, R. (2009). Automated analysis of behavior in zebrafish larvae. Behav. Brain Res. *203*, 127–136. https://doi.org/10.1016/j.bbr.2009.04.030.
81. Haase, R., Royer, L.A., Steinbach, P., Schmidt, D., Dibrov, A., Schmidt, U., Weigert, M., Maghelli, N., Tomancak, P., Jug, F., and Myers, E.W. (2020). CLIJ: GPU-accelerated image processing for everyone. Nat. Methods *17*, 5–6. https://doi.org/10.1038/s41592-019-0650-1.
82. van der Walt, S., Schönberger, J.L., Nunez-Iglesias, J., Boulogne, F., Warner, J.D., Yager, N., Gouillart, E., and Yu, T.; scikit-image contributors (2014). scikit-image: image processing in Python. PeerJ *2*, e453. https://doi.org/10.7717/peerj.453.
83. Bradski, G. (2000). The OpenCV library. Dr. Dobb's J. *25*, 120.

STAR★METHODS

KEY RESOURCES TABLE

REAGENT or RESOURCE	SOURCE	IDENTIFIER
Antibodies		
AP-conjugated anti-DIG Fab fragment	Roche	Cat#11093274910
Bacterial and virus strains		
Stellar Competent Cells	Clontech	Cat#636763
Chemicals, peptides, and recombinant proteins		
CF488A conjugated α-Bungarotoxin	Biotium	Cat#00005-100ug
Experimental models: organisms/strains		
AB	EZRC	Cat#1175
Tg[*mnx1En:bPAC-egfp*]	This paper	fu193
Tg[*mnx1:Gal4*]	Zelenchuk et al.[44]	N/A
Tg[*UAS:ChR2-P2A-dTomato*]	This paper	fu194
Tg[*UAS:bPAC-V2A-mCherry*]	Xiao et al.[42]	N/A
cpe Δ277	This paper	fu195
tac1 Δ564	This paper	fu196
Oligonucleotides		
See Table S1		N/A
Recombinant DNA		
Plasmid: Tol2-mnx1En:bPAC-egfp-polyA (pHD5)	This paper	N/A
Plasmid: Tol2-UAS-ChR2-P2A-dTomato-polyA	Soojin Ryu (Johannes Gutenberg University, Mainz) and this paper	N/A
Plasmid: cpe_Ribo2 (pHD18)	This paper	N/A
Plasmid: tac1_Ribo (pHD25)	This paper	N/A
Software and algorithms		
ImageJ	Schindelin et al.[70]	https://fiji.sc/
Zebrafish Tracking Software	This paper	https://github.com/MariusSeidenthal/zebrafish_angle_analysis

RESOURCE AVAILABILITY

Lead contact

Any additional information and requests for resources should be directed to and will be fulfilled by the lead contact, Alexander Gottschalk (a.gottschalk@em.uni-frankfurt.de).

Materials availability

All materials generated in this study are available on request from the lead contact.

Data and code availability

All python code generated in this study is publicly available via https://github.com as described in the key resources table.

EXPERIMENTAL MODEL AND STUDY PARTICIPANT DETAILS

Zebrafish maintenance and breeding

Adult zebrafish (*Danio rerio*) were maintained in groups inside 6 L tanks (5–7 fish per liter) located in a circulating water system (Zebcare, Nederweert, The Netherlands) with a 14 h/10 h light/dark cycle and in accordance with FELASA guidelines.[71] Prior to all optogenetic experiments zebrafish embryos were kept in E3 medium in an incubator at 28°C and total darkness. Developmental stages of embryos were determined as

described.[72] All experiments employing animals were conducted according to the European Directive 2010/63/EU on the protection of animals used for scientific purposes and the animal research board of the State of Hessen (animal protocol approval number V54-19c20/15-FR/1017, V54-19c20/15-FU/Anz. 1018, V54-19c20/15-FR/1019, and V54-19c20/15-FR/2003).

METHODS DETAILS

Molecular biology

To obtain the Tol2-mnx1En:bPAC-egfp-polyA plasmid (pHD5) the coding sequence of bPAC was amplified with primers bPAC-attB1-F (GGGGACAAGTTTGTACAAAAAAGCAGGCTGCGCCACCATGATGAAGCGG CTGGTGTA) and bPAC-attB2-R (GGGGACCACTTTGTA CAAGAAAGCTGGGTAGTACGTCCGCGGCTT GTCGTTT) and subjected to a Gateway BP-reaction (Thermo Fisher Scientific, Waltham, USA) with donor vector pDONR221 resulting in the middle entry clone pME-bPAC (pHD1). The middle entry clone (pHD1) was used in an Gateway LR-reaction together with the p5E-mnx1En,[44] p3E-polyA and the pDestTol2CG clones.[73] Furthermore, the plasmid Tol2-UAS-ChR2-P2A-dTomato-polyA, a gift from Dr. Soojin Ryu (Johannes Gutenberg University, Mainz) was used to generate the Tg[*UAS:ChR2-P2A-dTomato*] zebrafish line after sequence validation.

Templates for transcription of antisense *in situ* probes were amplified from 24 hpf cDNA by using specific PCR primers cpe_F_2 (CCCATCTCAAACGCCTCTGT), cpe_R_2 (ATAAGTCTGGACGCAGTGCC), tac1_F (GATGGGGAAACGGTCCTCTG) and tac1_R (GCG CAGGACTGTCGGTATTA). PCR products were cloned into the pCRII-TOPO vector (Thermo Fisher Scientific, Waltham, USA). Resulting plasmids cpe_Ribo2 (pHD18) and tac1_Ribo (pHD25) were transcribed with Sp6 or T7 RNA polymerase in a digoxigenin labeling reaction.

CRISPR/Cas9 target sites were identified and sgRNAs designed as described in.[74] The following DNA oligos were used together with the DR274 plasmid to construct templates for sgRNA transcription: cpe_Oligo_1-1 (TAGGACAGCGCAGAAAACAGGA), cpe_Oligo_1–2 (AAACTCCTGTTTTCTGCGCTGT), cpe_Oligo_3-1 (TAGGGTCGCGAGCTGCTCGTGC), cpe_Oligo_3-2 (AAACGCACGAGCAGCTCGC GAC), tac1_Oligo_1-1 (TAGGAAGTAACTAAAGTTTAGA), tac1_Oligo_1–2 (AAACTCTAAACTTTAGTTA CTT), tac1_Oligo_2-1 TAGGATTT ATTTAACATGCTTA) and tac1_Oligo_2-2 (AAACTAAGCATGTTAAATA AAT). See also Table S1.

Whole mount *in situ* hybridization

Whole mount *in situ* hybridization was carried out as described previously.[75] In brief, after paraformaldehyde (Carl Roth, Karlsruhe, Germany) fixation embryos were stored in MetOH and subsequently rehydrated. Embryos were treated with Proteinase K (5 μg/mL) according to the developmental stage. Proteinase K treatment was followed by refixation in 4% PFA for 20min. Unspecific RNA binding sites were blocked with Torula yeast RNA (Sigma-Aldrich, St. Louis, USA) before incubation with DIG-labelled RNA probes. Hybridization was carried out at 65°C overnight. To detect specifically bound RNA probes, embryos were incubated with AP-conjugated-*anti*-DIG antibodies (Roche, Basel, Switzerland) and stained with NBT/BCIP (Roche, Basel, Switzerland).

Microinjection of zebrafish embryos

In order to generate transgenic zebrafish lines, plasmid DNA was diluted to a final concentration of 12.5 ng/μL in water and approximately 0.5 nL were co-injected with *in vitro* transcribed *Tol2* mRNA (12.5 ng/μL) into 1-cell stage embryos. 2 dpf embryos were scored for expression of the *cmlc2:EGFP* transgenesis marker[73] and kept to establish the F0 generation.

To generate gene knockouts a pair of sgRNAs per gene (12.5 ng/μL each) were coinjected with Cas9 protein (Integrated DNA Technologies, Coralville, USA) as recommended by the manufacturer. After microinjection zebrafish embryos were kept in E3 medium in an incubator at 28°C. Primary injected F0 animals were mated with AB wildtype partners to obtain the F1 generation.

Genotyping of adult zebrafish

Fin biopsies were taken from adult zebrafish and genotyping PCRs for the respective *cpe* or *tac1* knockout alleles performed on tissue lysates using the primers cpe_Geno_F (CAAATATATGTGACCCGTTCGTC), cpe_Geno_R (GGCGATCCTCCATTATTGATTGG), tac1_Geno_F3 (GCTCACCTCCTCTGACGTAA) and tac1_Geno_R2 (TGTGAAATGTCACTAACTTTGTTGC) with Phusion DNA Polymerase (Thermo Fisher Scientific, Waltham, USA). See also Table S1.

Genotyping of live zebrafish embryos

Genotyping of 48 hpf embryos was done as described in Lambert et al., 2018 (ref. 76). The chorion was removed manually and embryos loaded onto a microfluidic chip in E3 followed by agitation on a base unit (wFluidx, Salt Lake City, USA). 10 μL of E3, containing genetic material, was used as template for genotyping PCRs as described above. Subsequently, embryos were transferred to 24-well plates with fresh E3 to recover.

RT-PCR

Total RNA was chloroform/phenol isolated from brain tissue using Trizol (Thermo Fisher Scientific, Waltham, USA) and isopropanol precipitated. cDNA was synthesized from 700 ng of total RNA with SuperScript II Reverse Transcriptase (Thermo Fisher Scientific, Waltham, USA) and oligo(dT) primers. PCR was performed using Taq DNA Polymerase (NEB, Ipswich, USA) in a T100 Thermal Cycler (Bio-Rad, Hercules, USA). PCR products were visualized on a 1.5% agarose gel with ethidiumbromide staining. The following primer pairs were used for

PCR: tac1_Intron1_F (TTGACATTGCGGGTTGGAAG), tac1_Intron1_R (TGAATCCACTCATCCTGCGA), gapdh_F (TGTTCCAGTACGACTC CACC) and gapdh_R (GCCATACCAGTAAGCTTGCC). See also Table S1.

Quantitative RT-PCR

Total RNA was recovered from adult brain tissue by chloroform/phenol extraction using Trizol (Thermo Fisher Scientific, Waltham, USA) with subsequent isopropanol precipitation. cDNA was synthesized from 700 ng of total RNA with SuperScript II Reverse Transcriptase (Thermo Fisher Scientific, Waltham, USA) and oligo(dT) primers. Quantitative PCR was performed using the iTaq Universal SYBR Green Supermix (Bio-Rad, Hercules, USA) in a CFX Connect Real-Time cycler (Bio-Rad, Hercules, USA) as described in the respective manuals. The average Ct values of replicates were normalized to *gapdh* or *β-actin* to obtain ΔCt values. For relative expression analysis ΔΔCt values were calculated as described in Livak and Schmittgen, 2018 (ref. 77). The following primer pairs were used for quantitative PCR: cpe_qPCR_F2 (GGTCAACTACATAGAGCAGGTTCA), cpe_qPCR_R2 (CCAACAAGCGCCAGTAGTCA), tac1_qPCR_F2 (ATCGGTCTGATGGGGAAACG), tac1_qPCR_R2 (ACGACTCTGGCTCTTCTTGG), tac3a_qPCR_F (GGACTCATGGGTCGACGAAG), tac3a_qPCR_R (AACCCACGACGAAAC CTCAG), tac3b_qPCR_F2 (GCCCTCGACTACTCCTTCAC), tac3b_qPCR_R2 (GCCTCACGATTTATTCCTGTGC), tac4_qPCR_F2 (AAGAG GGGGATATCTGGACTGT), tac4_qPCR_R2 (ATTTCACCCTTGTTTCTTCTCCT), gapdh_qPCR_F (CAGGCATAATGGTTAAAGTTGGTA), gapdh_qPCR_R (CATGTAATCAAGGTCAATGAATGG), bactin_qPCR_F (GATCTTCACTCCCCTTGTTCA) and bactin_qPCR_R (GGCAGC GATTTCCTCATC).

α-Bungarotoxin staining

Larvae (4 dpf) were fixed with 4% paraformaldehyde in PBST at 4°C over night. Heads were cut off to allow diffusion into the tissue and larvae were briefly digested with collagenase (1 mg/mL) for 15 min. Staining of acetylcholine receptors was performed with 10 μg/mL CF488A conjugated α-Bungarotoxin (Biotrend, Cologne, Germany) in PBST complemented with 10% FCS and 1% DMSO.

Confocal laser scanning microscopy and image analysis

For imaging of chemically fixed samples, embryos or larvae were treated with 4% formaldehyde (Polysciences, Warrington, USA) in PBST at 4°C over night and mounted in 1.5% low melting point agarose (Thermo Fisher Scientific, Waltham, USA). *in vivo* imaging was performed on larvae embedded in 1.5% low melting point agarose in E3 medium supplemented with 4.2 g/L MS-222 (Sigma-Aldrich, St. Louis, USA). Confocal imaging was done with a Zeiss LSM 780 microscope using Plan-Apochromat 10x/0.3 Air or Plan-Apochromat 20x/0.8 Air objectives. Images were processed and particle analysis of α-Bungarotoxin stained samples was done with ImageJ.[70]

Bright-field microscopy

For analysis of mutant phenotypes, previously genotyped larvae (4 dpf) were chemically fixed with 4% paraformaldehyde (Carl Roth, Karlsruhe, Germany) in PBST at 4°C over night and mounted in 1.5% low melting point agarose (Thermo Fisher Scientific, Waltham, USA). After *in situ* hybridization staining embryos were mounted in 100% glycerol (Carl Roth, Karlsruhe, Germany). Images of both sample types were taken with a Leica M205 FCA Stereomicroscope (Leica Microsystems, Wetzlar, Germany).

Zebrafish behavioral assays

For all behavioral experiments all embryos were kept in E3 medium and total darkness at 28°C previous to the assay. Animals were selected for the respective fluorescence marker with a Leica MZ16F stereomicroscope the day before the experiment. All assays were conducted at room temperature in pre-warmed E3.

Evoked tail-coiling

At 24 hpf ~15–20 embryos were transferred to a 6 cm Petri dish and the tail-coiling behavior monitored for 30 s before and 30 s during the exposure to blue LED light (470 nm, 0.1 mW/mm^2). In all behavioral assays, to stimulate bPAC as well as the wildtype control continuous blue light was applied. To activate ChR2 20 Hz light pulses (25 ms pulse length) were used. Videos were captured with an infrared background illumination at 30 frames per second for 1 min on a similar video recording assembly as described in Swierczek et al., 2011 (ref. 78). Spontaneous and evoked tail movements (STMs) were identified by a previously described MATLAB application.[79]

Tail-beat-assay with immobilized larvae

Zebrafish larvae at an age of 4 dpf were mounted in 1.5% low melting point agarose (Thermo Fisher Scientific, Waltham, USA) and covered with E3. Agarose around the tail was removed with a scalpel and the tail remained free to perform tail beat movements. Animals were kept in the dark for 10 s followed by a 10 s blue light illumination period (460 nm LED, 0.1 mW/mm^2). Videos were recorded with an Evolve Delta camera (Teledyne Photometrics, Tucson, USA) at a frame rate of 60 fps on a Zeiss Observer Z1 microscope equipped with an EC Plan-Neofluar 1x/0.025 M27 objective and red background illumination. The maximum angels between body axis and tail tip were extracted manually from minimum intensity projections in ImageJ.

Swimming assay

For analysis of swimming behavior, single animals at 4 dpf were transferred to an agarose arena with a diameter of 3 cm filled with E3 medium and adapted for 2 min under dark conditions. Videos were taken as described above with a frame rate of 30 fps. Video files of swimming behavior were recorded for 20 s. After a dark phase of 5 s, continuous or 20 Hz blue light (470 nm, 0.1 mW/mm^2) was applied from an LED ring for 10 s. Larvae were tracked with a custom macro in ImageJ (version 1.52). For each video frame pigmentation was smoothed by median filtering, animals separated from the background by thresholding and center of mass identified to obtain X- and Y-coordinates (as described in[80,81]). Distance traveled between consecutive video frames was calculated in pixels and converted into swimming speed in mm/s according to the size standard in Microsoft Excel.

Analysis of head-tail angles in freely behaving larvae

A custom written python script was used to analyze the tail bending angle of single freely swimming zebrafish larvae (https://github.com/MariusSeidenthal/zebrafish_angle_analysis). In short, this script applies a background correction to remove artifacts and detect the shape of the animal.[82] This is then skeletonized to a one-pixel line along the middle part of the body. The head is differentiated from the tail by analysis of surrounding pixel density in the binary image.[83] A single angle is then calculated between three points of the skeleton approximately corresponding to the tail tip, swim bladder and one point halfway between those.

Electrophysiology

Zebrafish larvae 4 dpf were used for electrophysiological recordings. Experiments were performed in a darkened room with the light of the stereomicroscope (used for dissection) and on the microscope used for patch clamp recordings being covered with red filter foil to avoid prestimulation of bPAC as much as possible. A single zebrafish larva was transferred to bathe solution (see below) containing tricaine (0.02%, MS222, Sigma Aldrich) for 1 min to anesthetize it for dissection. Under a stereomicroscope (Stemi 2000, Zeiss, Germany) the larva was decapitated with a scalpel and then transferred to a recording chamber coated with Sylgard 184 (Dow Silicones Corporation, USA). It was fixed on its side with two tungsten pins through the notochord. The skin on the top was peeled off with a fine forceps to allow access to the underlying muscle cells. The recording chamber was then placed on an Axioskop 2 FS Plus microscope (Zeiss, Germany) equipped with DIC optics and a 40x water immersion objective. Electrodes for whole-cell muscle recordings were pulled to an outer diameter of 2–3 µm (resistance ~5 MΩ) and lightly fire-polished using a Microforge MF-830 (Narishige, Japan). Bath solution (in mM): 134 NaCl, 2.9 KCl, 2.1 $CaCl_2$, 1.2 $MgCl_2$, 10 glucose, 10 Na-HEPES (pH 7.8). Intracellular solution (in mM): 120 KCl, 10 K-HEPES, 5 BAPTA (pH 7.4). Patch-clamp recordings were performed at room temperature using an EPC-10 amplifier (HEKA Elektronik, Germany). Data were acquired using the Patchmaster software (HEKA Elektronik, Germany) at a holding potential of −60 mV and filtered at 2.9 kHz bPAC photostimulation was performed using a KSL-70 LED light (Rapp Optoelectronics, 470 nm), triggered by the Patchmaster software. Miniature EPCs (mEPCs) were analyzed using Easy Electrophysiology software (https://www.easyelectrophysiology.com/).

QUANTIFICATION AND STATISTICAL ANALYSIS

Generally, data are shown as mean ± s.e.m., unless otherwise stated, and n indicates the number of animals tested. Statistical significance between groups was determined by Student's t test, Kruskal-Wallis test with Dunn post-hoc-test, 1-Way-ANOVA with Tukey multiple comparison of means or two-Way ANOVA with Tukey multiple comparison of means. The respective statistical test used is indicated in the figure legends. Data were analyzed and plotted with GraphPad Prism (GraphPad Software, version 8.02), Origin Pro 2023 (OriginLab) or the R statistical software environment (https://www.r-project.org/). Significance codes: '*' $p < 0.05$, '**' $p < 0.01$, '***' $p < 0.001$, '****' $p < 0.0001$).